



A Photonic Crystal Fiber-Based Biosensor with Quasi-D-shaped Layout and ITO-Graphene Combination

Jiaguo Tian¹ · Cheng Xu¹ · Songya Cui¹ · Lei Ma² · Yongqi Fu¹

Received: 11 August 2020 / Accepted: 25 November 2020 / Published online: 19 March 2021
© Springer Science+Business Media, LLC, part of Springer Nature 2021

Abstract

A quasi-D-shaped photonic crystal fiber (PCF) biosensor in the near-infrared region (NIR) is proposed for the purpose of detecting the analytes/liquids of different refractive indices (RIs) ranging from 1.21 to 1.32. In order to realize sensing in the near-infrared region, we use indium tin oxide (ITO) as the plasma material. Then a flake of graphene is deposited on the ITO film. Graphene has excellent molecular adsorption performance, which can improve the detection capability of the PCF sensor. Graphene becomes an ideal dielectric layer for sensing due to its large surface area and rich π -conjugation. To enhance the birefringence, we introduce two elliptical holes around the core. The proposed sensor is designed and numerically analyzed by finite element method. Thickness of the ITO, graphene layer, and the ellipticity of ellipse of PCF are varied so as to study its effect on the sensing characteristics of the proposed sensor. Wavelength sensitivity of the proposed sensor is as high as 12,000 nm/RIU (refractive index unit), and a maximum resolution can be 8.33×10^{-6} RIU. Compared with the traditional D-shaped sensors, the proposed sensor has the advantages of easy manufacturing and high sensitivity.

Keywords Photonic crystal fiber · Biosenor · Surface plasmon resonance

Introduction

Surface plasmon resonance (SPR) is widely used in the field of sensors. It has attracted the interest of many scholars in the past decade. The SPR sensor has great potential in the fields of medical diagnosis, biomolecular analyte detection, and organic chemistry detection [1–3]. Photonic crystal fibers are increasingly employed as the carrier of SPR sensors because of its flexible structure design and high birefringence. For example, Juan Liu designed a PCF-SPR sensor with a silver core [4]. The average wavelength sensitivity of this sensor can reach to the value of 23,821 nm/refractive index unit

(RIU) with a resolution of 4.2×10^{-6} RIU for an analyte refractive index (RI) ranging from 1.38 to 1.44. However, it is a technical challenge to deposit a silver film in the air hole of the PCF. Fengning Zha proposed a PCF-SPR sensor that has a detection for RI of the analyte ranging from 1.30 to 1.42 [5]. This sensor is structured with a D-shaped air hole inside the PCF, which increases the difficulty of processing. PCF is generally drawn at high temperature. However, how to make the D-shaped surface of the small hole smooth during the fabrication process is still a challenge at present. As all known, the smoothness of the coating plane seriously affects sensitivity of the sensor. In literature, the graphene-silver-based PCF-SPR sensor proposed by Ahmmed A. Rifat has a maximum amplitude sensitivity of 418 nm/RIU and resolution as high as 2.4×10^{-5} RIU [6]. However, the corresponding sensing range is as small as 1.46–1.49 only, and the detection range is too narrow to sense for practical applications. However, most of PCF-SPR sensors are applied to the detection of high refractive indexes. In practice, it is important to detect low refractive index analytes between 1.20 and 1.32, e.g., fluorine-containing organics, medical oxygen, liquid CO₂, and sevoflurane serving as anesthetics in the biomedical field [7, 8].

✉ Lei Ma
maleiii@aliyun.com

✉ Yongqi Fu
yqfu@uestc.edu.cn

Jiaguo Tian
shuishou320@163.com

¹ School of Physics, University of Electronic Science and Technology, Sichuan Province, Chengdu, People's Republic of China

² Jincheng College, Sichuan University, Sichuan Province, Chengdu, People's Republic of China

In this manuscript, we proposed a novel type of quasi-D-type PCF-SPR sensor coated with indium tin oxide (ITO) and a graphene layer. The operating range of the proposed sensor is in the IR region. The upward movement of the core allows us to polish away a small portion of the fiber only, which reduces the difficulty of manufacturing and increases the strength of the fiber. Generally speaking, gold and silver are commonly used for sensing materials. However, gold and silver have their SPR wavelength in the visible region. Gold is chemically stable and has a large shift in the resonance wavelength. But the refractive index change in this sensing area is a little [9]. Silver is a chemically active material and can be oxidized very quickly, which leads to degradation of its sensing performance [10]. Based on the reasons above, in this article we employ ITO as the sensing material. The plasma frequency of ITO can be tuned by means of changing the doping concentration of tin oxide to indium oxide to ensure that it works within the selected wavelength range [11, 12]. There are several advantages of choosing the working wavelength in the near-infrared region. Firstly, some proteins and biomolecules are marked in the NIR region. If the SPR-based sensing method is considered to detect such molecules, it is too difficult to use gold or silver as the sensing material. Secondly, the near-infrared evanescent wave can penetrate deeply into the analyte, which makes the high sensitivity. Finally, the fiber-based SPR sensor in NIR has low loss because of the low fiber transmission loss in this region. However, the ITO sensors cannot be used directly for biosensing because they do not have an ideal affinity for biomolecules. Therefore, we add a layer of graphene on its surface for the purpose of improving the affinity. As a new material, graphene is extensively explored by scholars [13–15]. Graphene can not only improve the performance of the sensor but also

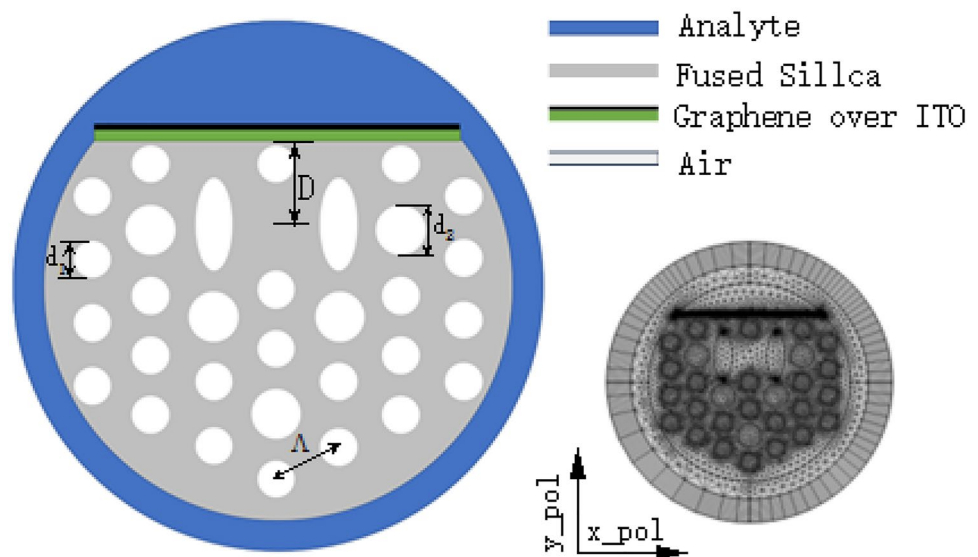
be helpful in significant adsorption of biomolecules due to $\pi-\pi$ stacking [16, 17].

A finite element method (FEM) is used to numerically analyze the performance of the D-shaped PCF-SPR sensor. Because the structure of the proposed sensor does not change in the z -direction (longitudinal), we built a two-dimensional model for our simulation. The establishment of a two-dimensional model also greatly reduces the running time of the calculation. By tuning the structural parameters, the maximum spectral sensitivity of up to 12,000 nm/RIU is obtained for analyte RIs ranging between 1.21 and 1.32, corresponding to the theoretical resolution of 8.33×10^{-6} RIU.

Structure Design and Numerical Simulation

In this article, we use the loss spectrum analysis method. Firstly, obtain the effective refractive index of the mode field according to the finite element method, and then draw the loss spectrum of the sensing model according to the imaginary part of the refractive index. In order to improve the calculation accuracy, the scattering boundary is fixed, and a perfectly matched layer (PML) is used to absorb the scattered energy. Figure 1 shows the schematic diagram of the PCF-SPR sensor based on fused silica. The diagram in the bottom right corner is the divided grid picture in the calculation, and the outermost layer is the perfect matching layer. Silica is set as the substrate material. The diameters of the big air hole and the small air hole are $d_1 = 1.2 \mu\text{m}$ and $d_2 = 1.6 \mu\text{m}$, respectively. The pitch of the adjacent air holes is $\Lambda = 1.8 \mu\text{m}$, and the polished depth $D = 4.6 \mu\text{m}$. There are two elliptical holes beside the core. The long axis length is $d_y = 1.5 \mu\text{m}$, the short axis length is $d_x = 0.6 \mu\text{m}$. ITO film is plated on the surface of

Fig. 1 Cross-section of schematic diagram of the proposed sensor



the optical fiber with a thickness of 45 nm. A monolayer of graphene is deposited on the ITO film with a thickness of 0.34 nm. The values of real and imaginary parts of the permittivity of ITO are calculated as [18]:

$$\epsilon_m(\lambda) = \epsilon_\infty - \frac{\lambda^2 \lambda_c}{\lambda_p^2(\lambda_c + i\lambda)} \tag{1}$$

where ϵ_∞ is the dielectric constant for the infinite value of the frequency, λ is the wavelength of the incident light, $\lambda_p = 5.6497 \text{ m} \times 10^7$ in the plasma wavelength of ITO, and $\lambda_c = 11.21076 \text{ m} \times 10^6$ in the collision wavelength of ITO.

Graphene is deposited on the ITO film. The complex RI of graphene can be obtained from the equation below [19]:

$$n_g = 3 + \frac{iC_1 \lambda}{3} \tag{2}$$

where constant C_1 is approximated as $5.446 \mu\text{m}^{-1}$ and λ is the vacuum wavelength in micrometer. The fixed thickness of single-layer graphene is 0.34 nm. Moreover, the total thickness of the graphene layer can be calculated using the following equation $t_g = 0.34\text{nm} \times L$, where L is the number of graphene layers.

Confinement loss is a basic parameter normally used for the purpose of estimating sensor performance, which can be obtained from the following equation [2, 20]:

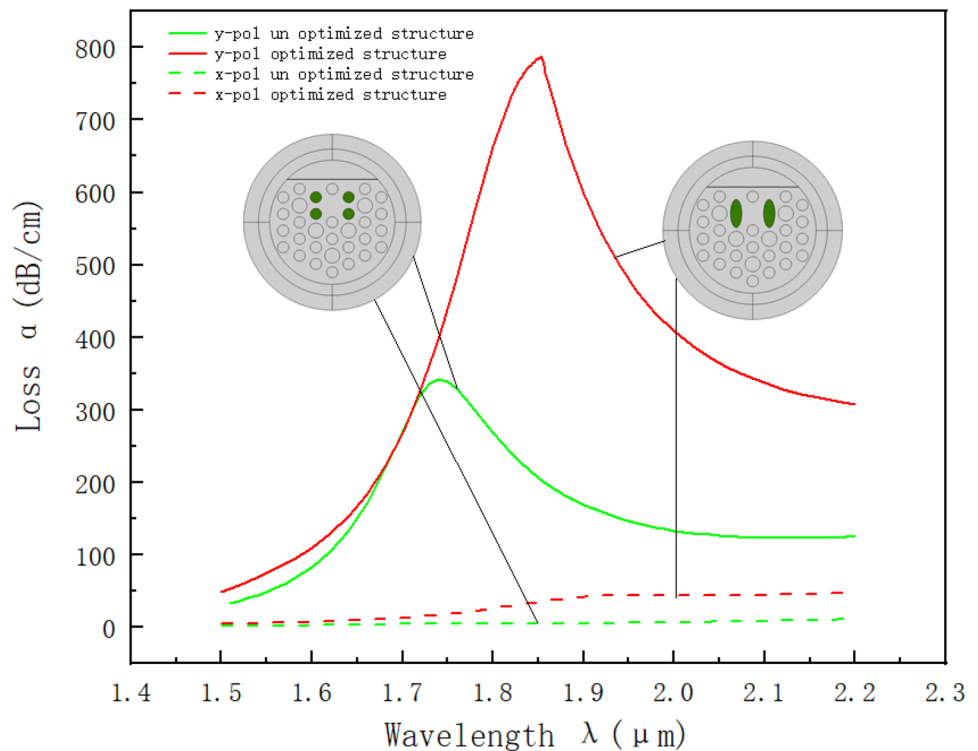
$$\alpha(\text{dB/cm}) = 8.686 \times k_0 \times \text{Im}(n_{\text{eff}}) \times 10^4 \tag{3}$$

where $k_0 = \lambda/2\pi$ is the wavenumber, here unit of λ is micrometers. $\text{Im}(n_{\text{eff}})$ represents the imaginary part of the effective refractive index. It can be known from Eq. (3) that the confinement loss is proportional to the imaginary part of the effective refractive index.

Here, we intentionally design the layout with two elliptical holes around the core for the purpose of destroying the symmetry and obtain a significant polarization effect. The length of long axis is d_y , the short axis is d_x , and the corresponding ellipticity $\eta = d_y/d_x$. As can be seen from Fig. 2, the green solid line and the dashed line, respectively, indicate the loss of y-pol and x-pol when the elliptical air holes are not introduced. The red solid line and the dashed line, respectively, represent the loss of y-pol and x-pol for the layout of the elliptical air holes. In comparison, it can be seen clearly that after the structure is improved, the polarization of the fundamental mode in the y-direction is nearly doubled, and the confinement loss is red-shifted. Confinement loss is one of the important parameters of the biosensors like PCF-SPR. The higher the loss, the easier of the sensor detection will be. At the same time, we can also see from Fig. 2 that the polarization loss of the fundamental mode in x-direction is extremely low. Thus, in this article, our study concentrates on the confinement loss of y-pol.

At present, the manufacturing and drawing technology of PCF are well developed [21, 22]. The manufacturing

Fig. 2 Confinement loss for before and after introducing the oval air holes with x direction (dashed) and y direction (solid)



technology of ITO film is also mature and has many applications in industry. In addition, it was reported that graphene can be deposited on ITO [23]. Therefore, we believed that the proposed quasi-D-shaped PCF-based SPR sensor can be practically realized.

Results and Discussion

In this section, we perform preliminary numerical calculations on the proposed structure. Various modes such as core-guided mode, surface plasmon polaritons (SPPs) mode, and coupled mode are shown in the figure below. Moreover, the relationship between confinement loss and dispersion is observed.

Loss Spectra and Dispersion Relations

We investigate the mechanism of plasma wave transduction in more detail in this sub-section. A typical fiber optical plasmonic sensor operates near the phase matching point between the core-guided mode and the metalized surface plasmon wave. We show the dispersion relationship between the core-guided mode (green curve) and the surface plasmon polaritons mode (SPPs mode, see blue curve), as shown in Fig. 3. The phase matching point is 1748 nm, at which the refractive index of the fundamental mode and the plasma mode are equal. Near the phase matching point, the effective refractive index of the fundamental mode has a sudden rise, while the effective refractive index of the plasma mode has a sudden drop. In

the vicinity of the phase matching point, the two modes are strongly mixed, as energy is transferred from the fundamental mode to the plasmonic mode, the loss of the fundamental mode increases dramatically. Confinement loss reaches its peak at this point, as shown by the red curve. Detecting the increase of confinement loss near the phase matching point has become the crucial issue for many sensor designs.

Sensitivity

The proposed sensor is surrounded by analyte, as shown in Fig. 1. Firstly, we review the principle of SPR sensor. When the propagation constant of the incident light is equal to the collective oscillation of electrons on the metal surface, their momentum can be matched and resonance occurs. Therefore, SPR is highly sensitive to changes of the refractive index (RI). When RI of the analyte changes, λ_{peak} has blue-shift or red-shift accordingly. Figure 4 shows the loss spectrum of the fundamental mode when the RI changes from 1.21 to 1.32. As shown in the pictures, as the RI increases, λ_{peak} moves toward the long wavelength direction, i.e., a red shift occurs. When the RI reaches 1.33, the loss peak is broadened, which is not easy to be measured and cannot meet the performance requirements of the sensor. Thus, it is not considered here. Wavelength sensitivity is one of the important parameters for analyzing sensor performance. The overall wavelength sensitivity can be estimated with the following formula [24]:

Fig. 3 Dispersion relation of the core-guided mode (green), plasmonic mode (blue), and the loss spectrum (red); inset of (a) shows the electric field of the plasmonic mode and inset of (b) shows the electric field of core-guided mode; (c) shows the electric field on the phase matching point with design parameters of $n_a = 1.31$, $d_x = 1.2 \mu\text{m}$, $d_y = 1.6 \mu\text{m}$, thickness of ITO = 45 nm, and number of graphene layer $L = 1$

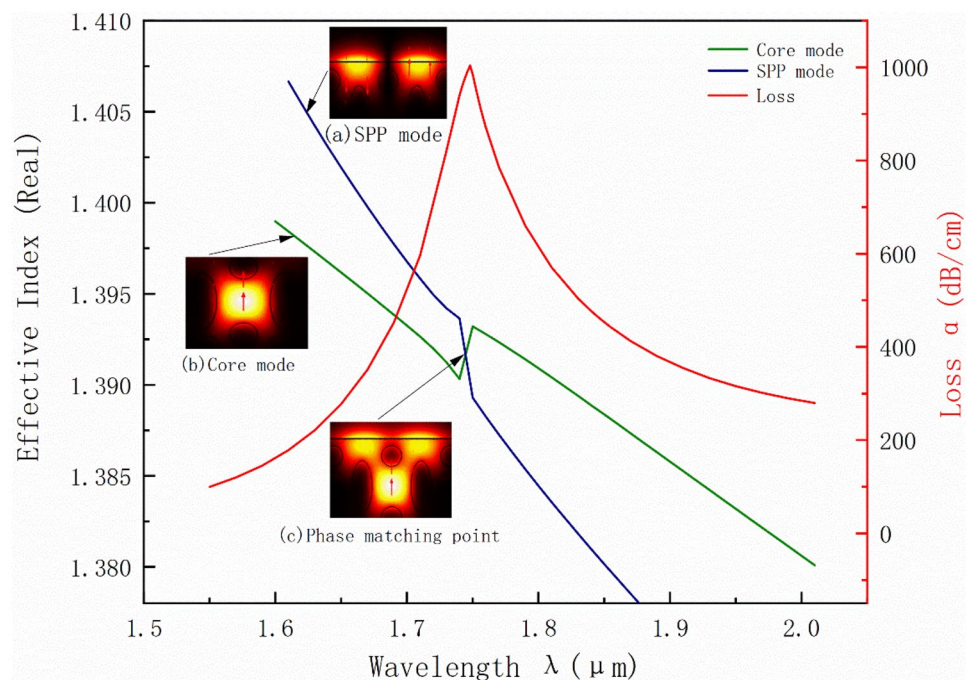
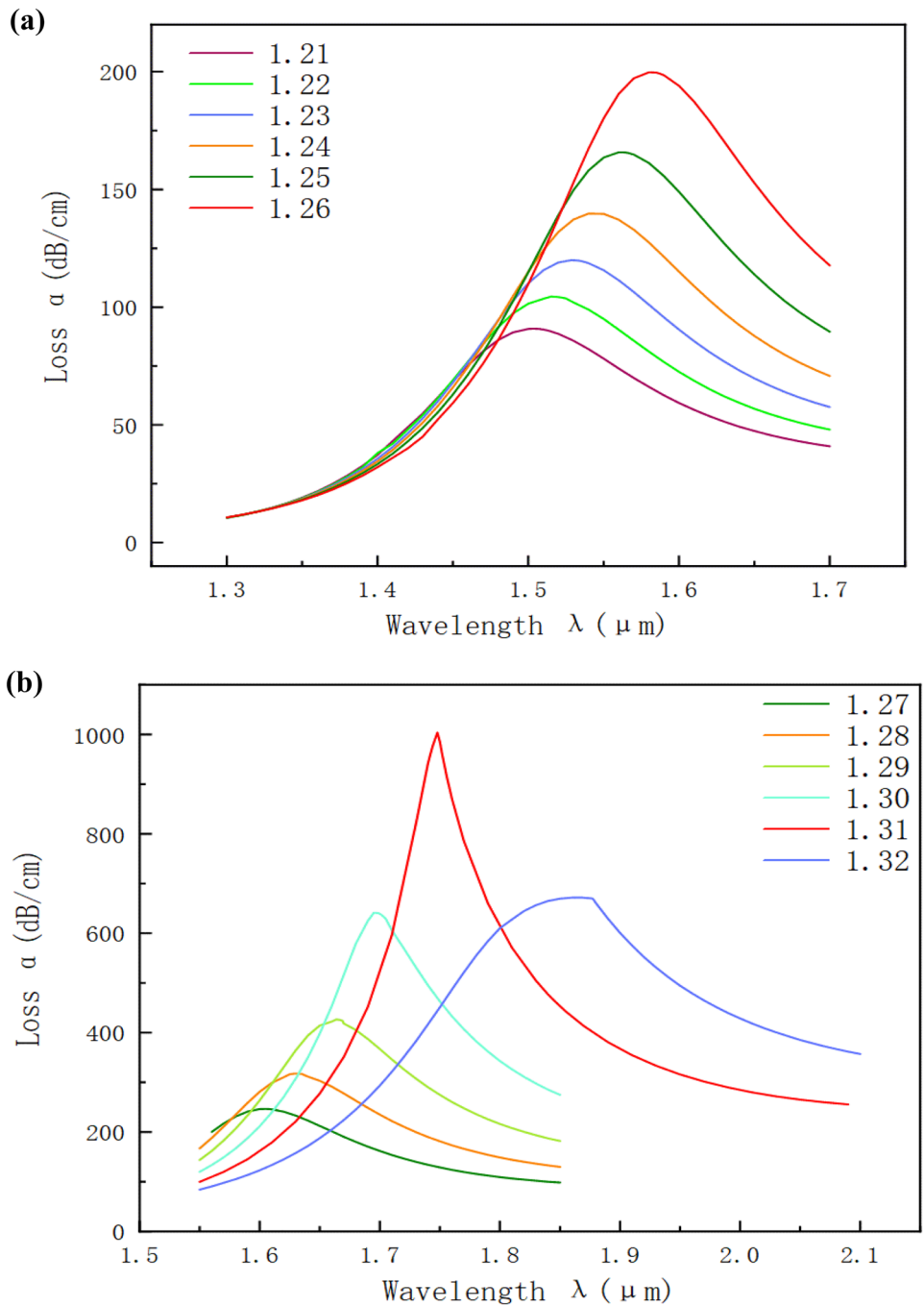


Fig. 4 Confinement loss spectrum of the sensor for RIs: **a** 1.21–1.26 and **b** 1.27–1.32, with the design parameters of $d_1 = 1.2 \mu\text{m}$, $d_2 = 1.6 \mu\text{m}$, $D = 4.6 \mu\text{m}$, $d_x = 0.6 \mu\text{m}$, $d_y = 1.5 \mu\text{m}$, $t_{\text{ITO}} = 45 \text{ nm}$, and $L = 1$



$$S(\text{nm}/\text{RIU}) = \frac{\Delta\lambda_{\text{peak}}}{\Delta n_a} \tag{4}$$

where Δn_a is the variation of analyte RIs and $\Delta\lambda_{\text{peak}}$ is the difference between the two resonance wavelengths. There is a maximum peak shift of $\Delta\lambda_{\text{peak}} = 120 \text{ nm}$ with RIs varying from 1.31 to 1.32, and a maximum spectral sensitivity of 12,000 nm/RIU is achieved. Resolution of a sensor is another important parameter, which can be expressed by the following equation [24]:

$$R(\text{RIU}) = \Delta n_a \frac{\Delta\lambda_{\text{min}}}{\Delta\lambda_{\text{peak}}} \tag{5}$$

where $\Delta\lambda_{\text{min}}$ is the resolution of the instrument, which is assumed to be 0.1, $\Delta\lambda_{\text{peak}}$ represents the difference of the wavelength peak shift, and Δn_a indicates the change in refractive index (0.01) of the analyte. When the RI of the analyte changes from 1.31 to 1.32, the resolution of this sensor reaches the value of $8.33 \times 10^{-6} \text{ RIU}$.

Furthermore, the comparison between the sensor we designed and the reported sensor is shown in Table 1. It can be seen from the table that our sensor is very competitive.

Investigation of Various Structural Parameters

As a type of microstructure fiber, the structure of PCF has a great influence on its performance. In this section, the influence of structural parameters of the quasi D-shaped PCF such as ellipse parameters, ITO layer thickness, and the number of graphene layer can be observed on the sensing performance of the proposed sensor.

Impact of the Parameters of Elliptical Holes on the Sensing Performance

In this section we discuss the influence of η of the elliptical hole surrounding the core on the performance of the proposed sensor. We know that η affects not only the birefringence of the structure but also the distribution of light transmission energy. Therefore, in order to obtain good polarization characteristics and effective transmission quality, it is necessary to optimize the size of the elliptical hole.

Figure 5 depicts the variation in the peak loss with different η . In order to change the ellipticity, we fix geometrical parameter of $d_x = 0.6 \mu\text{m}$ and only change d_y from 1.4 to 1.7 μm . As can be seen from Fig. 5a that when $d_x = 0.6 \mu\text{m}$ and $d_y = 1.5 \mu\text{m}$, the peak value of the confinement loss reaches the maximum value, and its peak loss is the sharpest. In the same way, we fix $d_y = 1.5 \mu\text{m}$ and change d_x from 0.4 to 0.7 μm , and we obtain the results, as shown in Fig. 6b. When $d_y = 1.5 \mu\text{m}$ and $d_x = 0.6 \mu\text{m}$, the confinement loss reaches the maximum value.

Impact of ITO Layer Thickness

In this section, we discuss the influence of ITO film thickness on sensor performance. The thickness of the ITO layer varies from 40 to 60 nm, and the maximum confinement loss occurs at 45 nm, as shown in Fig. 6. When the thickness exceeds this value, high damping loss can result in an overall reduction in confinement loss.

Impact of Graphene Layer Thickness

The number of graphene layers also greatly affects the performance of the sensor. As can be seen in Fig. 7, with the number of graphene layers increases from $L = 1$ to $L = 5$, the confinement loss decreases from 886 to 613 dB/cm accordingly. The reason is that as the number of graphene layers increases, the electronic behavior of graphene will approach to that of bulk graphite according to the infrared conductivity spectrum mentioned in the literature [29].

Impact of Polishing Depth

The smooth sensing surface of the D-shaped sensor can be manufactured by means of polishing; hence, the impact of the polishing depth on the performance of the sensor also needs to be considered here. Figure 8 shows the loss spectrum when the polishing depth d changes from 2.7 to 2.9 μm . It can be seen from the figure that the peak value reaches the highest point in the case of $d = 2.8 \mu\text{m}$.

Conclusions

A highly sensitive biosensor designed on the basis of graphene layers coated with ITO layer structured in quasi-D-shaped is proposed. In order to achieve the desired performance, we optimize the sensor structure parameters. The advantage of using ITO is that its resonance wavelength can be tuned in the near-infrared regime, and graphene layers ensure the affinity of the sensor for biomolecules. The structure is numerically analyzed using a finite element method. The resolution of the proposed sensor can reach to the level of 8.33×10^{-6} RIU, with wavelength sensitivity of as high as 12,000 nm RIU⁻¹ for RI variation of the analytes ranging from 1.21 to 1.32. The sensor has excellent sensing performance and huge commercial potential in biosensing and environmental monitoring. At the same time, it should be noted that this type of sensor (including our proposed) cannot obtain excellent sensing performance in the entire effective sensing range. This should be the direction of our future work.

Table 1 Comparative analysis of previously reported RI sensor

Structural characteristics with references	RI range	Max. Wav. Sens (nm/RIU)	Resolution (RIU)
Graphene-based quasi-D-shaped sensor [25]	1.33–1.38	10,693	9.35×10^{-6}
Graphene-based D-shaped SPR sensor [19]	1.33–1.35	5700	1.754×10^{-5}
Graphene-gold deposited sensor [26]	1.33–1.39	4391	2.284×10^{-5}
D-shaped sensor coated with ITO [27]	1.28–1.34	6000	1.67×10^{-5}
Silver-graphene based D-shaped biosensor [28]	1.34–1.40	4850	2×10^{-5}
Our proposed sensor	1.21–1.32	12,000	8.33×10^{-6}

Fig. 5 Confinement loss for different ellipticities of elliptical holes. **a** Fix d_x and change d_y from 1.4 μm to 1.7 μm . **b** Fix d_y and change d_x from 0.4 to 0.7 μm

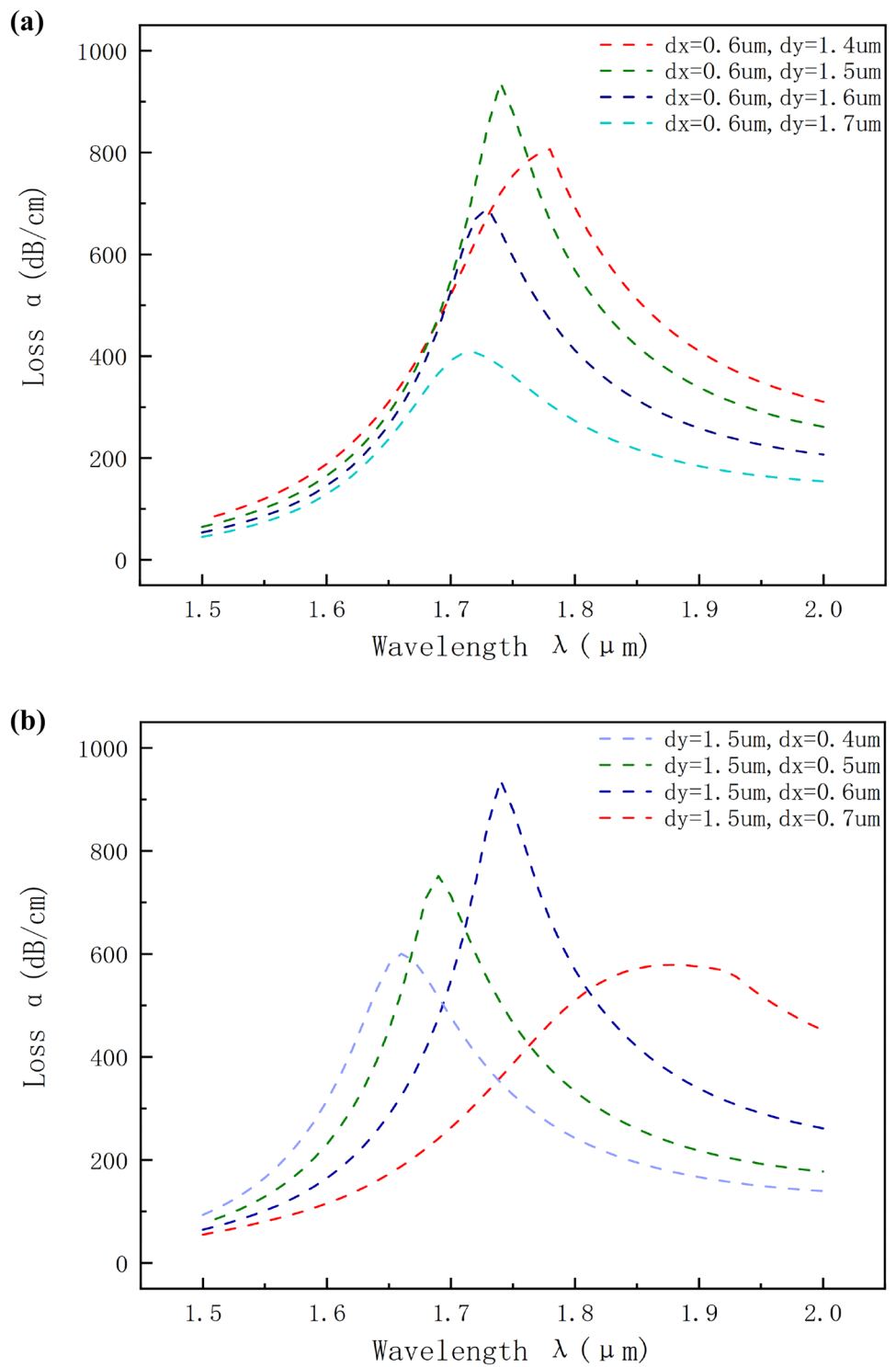


Fig. 6 Variation of confinement loss with different ITO thickness

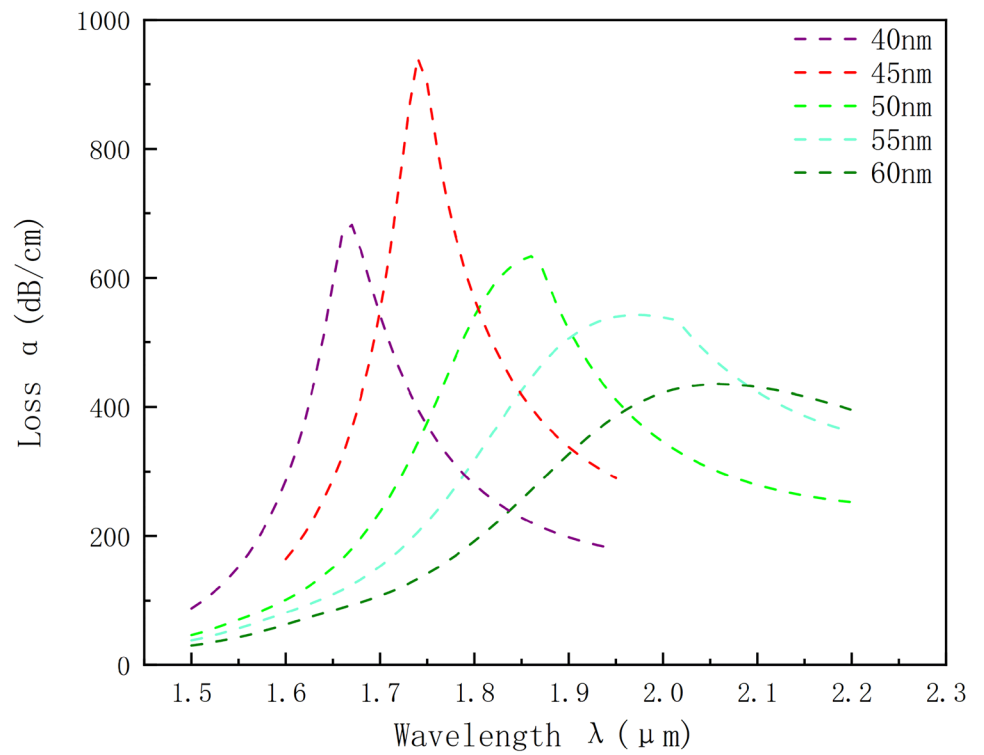


Fig. 7 Variation of loss peaks with varying the number of graphene layer

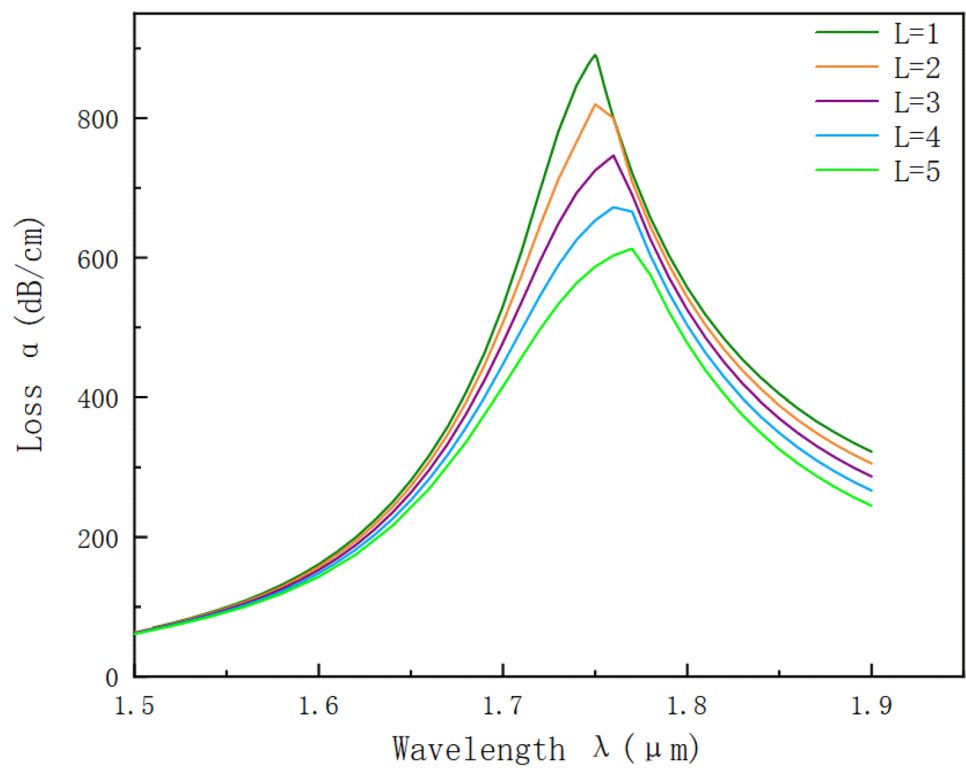
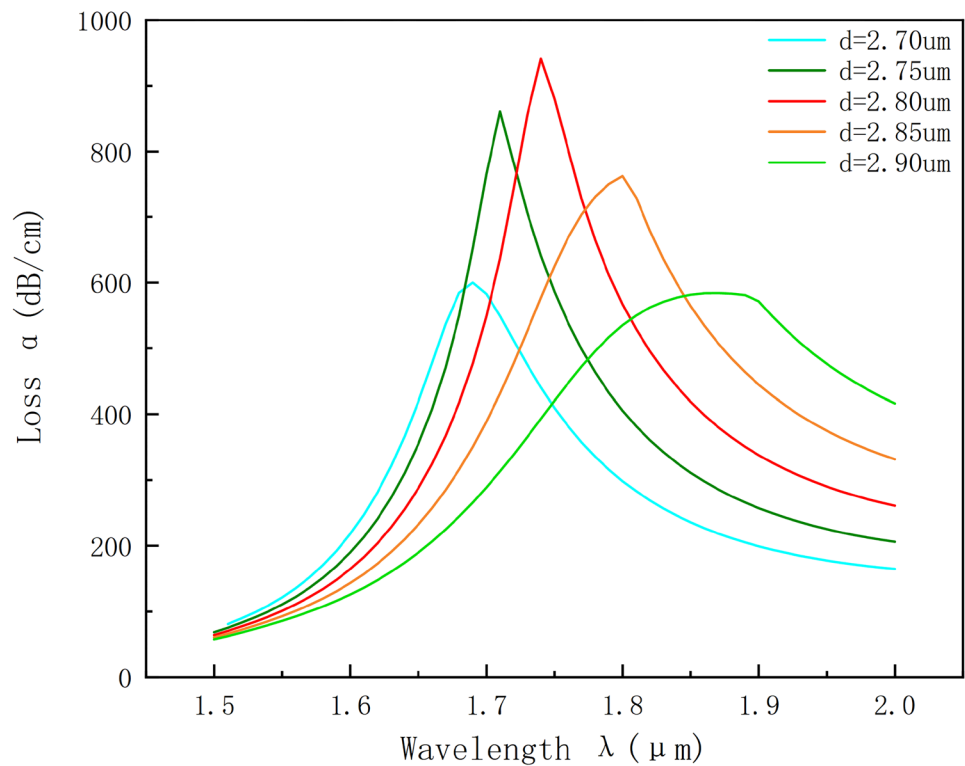


Fig. 8 Variation of loss with different polishing depths



Authors' Contributions All authors contributed to the study conception and design. Material preparation, data collection, and analysis were performed by Jianguo Tian, Cheng Xu, and Songya Cui. The first draft of the manuscript was written by Jianguo Tian. The revision of the manuscript was completed by Jianguo Tian and Yongqi Fu. All authors read and approved the final manuscript.

Data Availability All data generated or analyzed during this study are included in this published article.

Compliance with Ethical Standards

Competing Interests The authors declare that they have no conflict of interest.

Ethical Approval This research is an original research, and there is no plagiarism from others.

Consent to Participate Informed consent was obtained from all individual participants included in the study.

Consent to Publish The participant has consented to the submission of the case report to the journal.

References

- Liang G, Luo Z, Liu K, Wang Y, Dai J, Duan Y et al (2016) Fiber optic surface plasmon resonance-based biosensor technique: fabrication, advancement, and Application, *Crit Rev Anal Chem* 46:213–223
- Islam MS, Cordeiro CMB, Sultana J, Aoni RA, Feng S, Ahmed R, Dorraki M, Dinovitsner A, Ng BW-H, Abbott D et al (2019) A Hi-Bi ultra-sensitive surface plasmon resonance fiber sensor. *IEEE Access* 7:79085–79094
- Rifat AA, Mahdiraji GA, Shee YG, Shawon MJ, Adikan FRM et al (2016) A Novel Photonic Crystal Fiber Biosensor Using Surface Plasmon Resonance. *Procedia Engineering* 140:1–7
- Liu J, Liang H-Q, Liu B, He X-D, Chen Z-P et al (2019) Abnormal sensing properties of surface plasmon resonance sensor based on photonic crystal fibers. *Optical Fiber Technology* 48:248–252
- Zha F, JL, Sun P, Ma H et al (2018) Highly sensitive selectively coated D-shape photonic crystal fibers for surface plasmon resonance sensing. *Physics Letters A*
- Rifat AA, Mahdiraji GA, Chow DM, Shee YG et al (2015) Photonic crystal fiber-based surface plasmon resonance sensor with selective analyte channels and graphene-silver deposited core. *Sensors* 15:11499–11510
- Yang Z, Xia L, Li C, Chen X, Liu D et al (2019) A surface plasmon resonance sensor based on concave-shaped photonic crystal fiber for low refractive index detection. *Optics Communications* 430:195–203
- Haque E, Mahmuda S, Hossain MA, Hai NH, Namihira Y, Ahmed F et al (2019) Highly sensitive dual-core PCF based plasmonic refractive index sensor for low refractive index detection. *IEEE Photonics J* 11:1–9
- Verma RK, Gupta BD (2010) Surface plasmon resonance based fiber optic sensor for the IR region using a conducting metal oxide film. *Optical Society of America*
- Zhang HK, Zhou C, Song P, Wang J, Zhu CG, Wang PP (2018) Silver layer thickness insensitive index sensor based on hollow core photonic crystal fiber. *Optik* 160:333–339
- Franzen S (2008) Surface plasmon polaritons and screened plasma absorption in indium tin oxide compared to silver and gold. *American Chemical Society*

12. Rhodes C, Cerruti M, Efremenko A, Losego M, Aspnes DE, Maria JP, Franzen S et al (2008) Dependence of plasmon polaritons on the thickness of indium tin oxide thin films. *J Appl Phys* 103
13. Tiwari JN, Chang YM, Tiwari RN, Lin KL et al (2010) A promising approach to the synthesis of 3D nanoporous graphitic carbon as a unique electrocatalyst support for methanol oxidation
14. KCK, Tiwari JN, Nath K, Tiwari RN, Nam HG, Kim KS et al (2013) Interconnected Pt-nanodendrite/DNA/reduced-graphene-oxide hybrid showing remarkable oxygen reduction activity and stability
15. NKD, Tiwari JN, Park HJ, Sultan S, Kim MG, Haiyan J, Lee Z, Kim KS et al (2020) Remarkably enhanced catalytic activity by the synergistic effect of palladium single atoms and palladium-cobalt phosphide nanoparticles. *Nano Energy*
16. Rifat AA, Mahdiraji GA, Ahmed R, Chow DM, Sua YM, Shee YG, Adikan FRM et al (2016) Copper-graphene-based photonic crystal fiber plasmonic biosensor. *IEEE Photonics J* 8:1–8
17. Nayak JK, Jha R (2017) Numerical simulation on the performance analysis of a graphene-coated optical fiber plasmonic sensor at anti-crossing. *Appl Opt* 56:3510–3517
18. Singh S, Gupta BD (2010) Simulation of a surface plasmon resonance-based fiber-optic sensor for gas sensing in visible range using films of nanocomposites. *Measurement Science and Technology* 21
19. Patnaik A, Senthilnathan K, Jha R et al (2015) Graphene-based conducting metal oxide coated D-Shaped Optical Fiber SPR Sensor, *IEEE Photonics Technology Letters*
20. Chu S, Nakkeeran K, Abobaker AM, Aphale SS, Babu PR, Senthilnathan K et al (2019) Design and Analysis of Surface-Plasmon-Resonance-Based Photonic Quasi-Crystal Fiber Biosensor for High-Refractive-Index Liquid Analytes. *IEEE Journal of Selected Topics in Quantum Electronics* 25:1–9
21. Chen Y, Xie Q, Li X, Zhou H, Hong X, Geng Y et al (2017) Experimental realization of D-shaped photonic crystal fiber SPR sensor. *Journal of Physics D: Applied Physics* 50
22. Guiyao Z, Zhiyun H, Shuguang L, Lantian H et al (2006) Fabrication of glass photonic crystal fibers with a die-cast process. *Applied optics* 45:4433–4436
23. Singh DP, Gupta SK, Vimal T, Manohar R et al (2014) Dielectric, electro-optical, and photoluminescence characteristics of ferroelectric liquid crystals on a graphene-coated indium tin oxide substrate. *Phys Rev E Stat Nonlin Soft Matter Phys* 90:022501
24. Azab MY, Hameed MFO, Heikal AM, Swillam MA, Obayya SSA et al (2018) Design considerations of highly efficient D-shaped plasmonic biosensor. *Optical and Quantum Electronics*
25. SL, An G, Wang H, Zhang X, et al (2017) Metal Oxide-Graphene-Based Quasi-D-Shaped Optical Fiber Plasmonic Biosensor. *IEEE Photonics Journal* 9:1–9
26. SL, An G, Cheng T, Yan X, Zhang X, Zhou X, Yuan Z, (2018) Ultra-stable D-shaped Optical Fiber Refractive Index Sensor with Graphene-Gold Deposited Platform. *Plasmonics* 14:155–163
27. Huang T (2016) Highly sensitive SPR sensor based on D-shaped photonic crystal fiber coated with indium tin oxide at near-infrared wavelength. *Plasmonics* 12:583–588
28. FW, Tong K, Wang M, Dang P, Wang Y, Sun J, et al (2018) D-shaped photonic crystal fiber biosensor based on silver-graphene. *Optik* 168:467–474
29. Maka KF, Y.Sfeirb M, Misewichb JA, F.Heinz T et al (2010) The evolution of electronic structure in few-layer graphene revealed by optical spectroscopy. *Proceedings of the National Academy of Sciences*

Publisher's Note Springer Nature remains neutral with regard to jurisdictional claims in published maps and institutional affiliations.